applied sciences

MDPI

Article

Design of Non-Intrusive Online Monitoring System for Traction Elevators

Zhixing Li *, Jiahui Ning and Tianhao Li

School of Mechanical-Electronic and Vehicle Engineering, Beijing University of Civil Engineering and Architecture, Beijing 100044, China; jhning717@163.com (J.N.)
* Correspondence: onyxlzx@126.com

Abstract: With the increase in elevator usage, more and more elevator real-time monitoring equipment is being applied to the operation of elevators. Traditional elevator monitoring equipment adopts a multi-sensor decentralized installation and layout, and the monitoring accuracy is low, which directly affects the effective alarm of the monitoring system; however, existing online monitoring systems cannot quickly alarm for faults. Aiming to solve the above problems, an elevator online monitoring system based on narrow-band Internet of Things (NB-IoT) is designed. The system is highly integrated with an STM32 main control chip, a six-axis acceleration gyroscope sensor, and an air pressure sensor to realize the edge calculation of the monitoring system. At the same time, this paper eliminates the temperature drift of the pressure sensor by using a temperature compensation algorithm and inputs the extracted characteristic parameters into the BP neural network for training to eliminate the zero drift so as to obtain the real-time height data of the elevator. The six-axis acceleration gyroscope sensor is used to calculate the posture so as to avoid the problem that a three-axis acceleration sensor or a three-axis gyroscope sensor alone cannot obtain accurate posture data. In order to further improve the monitoring accuracy, the peak-to-peak value of the signal is calculated by using a 95% confidence interval algorithm to reduce the suppression of the high-frequency components of the signal by noise and ensure that the signal has a large signal-to-noise ratio so that the obtained elevator car posture and vibration operation data are more accurate. Finally, the effectiveness of the proposed method is verified by experiments.

Keywords: NB-IoT; elevator monitoring; highly integrated; BP neural network

check for updates

Citation: Li, Z.; Ning, J.; Li, T. Design of Non-Intrusive Online Monitoring System for Traction Elevators. *Appl. Sci.* **2024**, *14*, 4346. https://doi.org/10.3390/app14114346

Academic Editor: Subhas Mukhopadhyay

Received: 23 January 2024
Revised: 20 February 2024
Accepted: 26 February 2024
Published: 21 May 2024

1. Introduction

According to statistics, there were 23 elevator accidents and 17 deaths nationwide in 2021, accounting for 20.91% of the total number of special equipment accidents in 2021 [1]. After an elevator is activated, routine maintenance of the elevator is very important. Along with the growing length of time of an elevator's use, the mechanical devices inside it are bound to age. If the daily maintenance of an elevator is not in place, the elevator will exhibit safety hazards, thus reducing the reliability of the elevator, and when the elevator is not maintained for a long time or maintenance is not in place, it may also lead to serious personal injury accidents. In order to avoid the occurrence of the above situation, elevator maintenance companies should always be aware of the real-time operation of their elevators. Currently, the main maintenance method is regular maintenance, and this is inefficient for maintenance personnel. Using "Internet +" thinking, an elevator online monitoring platform was designed, realizing the real-time status of elevator online monitoring, daily maintenance unified scheduling, maintenance-task-centralized management, and fault information emergency alarms [2] so that an elevator maintenance company can know an elevator's running status in real-time, check an elevator's failure trend, improve the efficiency of elevator maintenance, and reduce the occurrence of elevator accidents, and after the occurrence of elevator accidents, the maintenance company can always know

the real-time running status of the elevator and check the failure trend of the elevator. This can improve the efficiency of elevator maintenance, reduce the incidence of elevator accidents, allow personnel to arrive at the scene in time to deal with elevator accidents, and scientifically arrange the repair method and maintenance time of each elevator. At present, safety accidents in elevators are a very pressing issue, and it is necessary to design a set of elevator condition monitoring systems for elevator mechanical failures.

Vibration and pressure pulsation peak-to-peak values are important indicators in elevator condition monitoring and fault diagnosis. The main basis for the stable operation of elevators is the peak-to-peak values of vibration measurement points in the national standards GB/T 6075.5-2002 [3] and GB/T 11348.5-2002 [4] and the international standards ISO 10816.5-2000 [5] and ISO 20816-5-2018 [6]. However, the above standards only provide a peak-to-peak value calculation method without noise interference, but actual vibration signals are inevitably affected by noise interference, and the relevant standards do not explain how to calculate the peak-to-peak values in this case. Fei Zhang et al. [7,8] have systematically summarized the problems related to the calculation of peak-to-peak values under steady-state and transient operating conditions. At present, there is no doubt about the selection of the number of cycles for peak-to-peak value calculation under steady-state conditions, and the latest revised standards, GB/T 17189-2017 [9], IEC 60994 [10], and ISO 20816-2017 [11], require that the number of calculation cycles not be less than 8 or 10, and Fei Zhang et al. [7] show that the number of cycles should not be less than 6 under steady-state conditions through a study of related cases. The literature shows that the number of cycles should not be less than six under steady-state conditions through relevant case studies. However, in the process of revising the existing standards, the relevant experts' disagreement mainly focuses on what confidence interval values are used to calculate the peak-to-peak values, including three confidence intervals of 97.5%, 97%, and 95%. Appendix E of the latest revision of ISO 20816 [6] recommends the use of 95% confidence intervals, and this method is briefly validated using simulated and measured signals. However, this validation is not perfect; for example, the signal-to-noise ratio of the signal is not fully considered, and the signal is not obtained based on quasi-periodic sampling. For the above problems, this paper adopts the 95% confidence interval algorithm to calculate the peak-to-peak value of the signal in order to alleviate the suppression of the high-frequency components of the signal by noise. At the same time, in order to avoid the problem of using three-axis acceleration data for posture solving, which cannot be used to obtain the heading angle, and the problem that the use of three-axis gyroscope data for calculating the posture of the car alone requires the time integration of the angular velocity, a six-axis acceleration gyroscope sensor is used to calculate the posture of the cabin. The results obtained from the two calculations are complementarily fused, thus further improving the monitoring of elevators by the designed system.

In addition, in the design of an elevator fault operation monitoring system, Liu Songguo et al. [12] designed a microprocessor-based monitoring system that uses multiple independent sensors to collect an elevator's operation status in real-time; Wang Enliang et al. [13] proposed the design of an elevator remote monitoring system based on a customized communication protocol; Chen Zhiping et al. [14] extracted characteristic parameters for elevator car vibration data and diagnosed elevator faults through big data analysis; Yang Yu et al. [15] designed a non-intrusive elevator operation state monitoring method to complete the tracking of real-time elevator positions by using the traceless Kalman filter algorithm, which integrates the synchronous positioning and map building techniques; Min Zhang et al. [16] used a wireless radio frequency system that is able to obtain and save an elevator's operation data in real-time; Sun Yuguo [17] designed a WiFi three-axis wireless vibration sensor that is able to directly transmit an elevator's vibration signals to the cloud platform to achieve remote data collection; Xu Jinhai et al. [18–20] analyzed the vibration signals of an elevator through the collection of data after the use of a variety of algorithms to monitor the elevator's fault information; Nakanishi et al. [21] used a GPS system and pressure sensor to calibrate the height signal; and Matyja et la. [22] used

temperature and humidity to correct the pressure sensor. Although the above monitoring techniques of an elevator's operating status have achieved certain results, the barometric pressure sensor applied in height monitoring is susceptible to data fluctuations due to environmental influences, and the barometric pressure sensor may produce zero drift in an environment with stable air pressure; if the use of other height monitoring techniques (GPS, laser, and radar) is too expensive, they are rarely considered. This paper is based on BP neural network training to eliminate the impact of the zero drift of a barometric pressure sensor on the height error so as to make an elevator's height monitoring more accurate and effective.

In summary, fault diagnosis systems for traction elevators have been widely used and have achieved remarkable results. However, previous studies are based on using sensors to collect data and using cloud servers for fault diagnosis. In this paper, a non-intrusive, online, height-integrated monitoring system for traction elevators, based on NB-IoT (Narrow Band Internet of Things) and STM32, is designed. The 95% confidence interval algorithm is used to calculate the peak-to-peak value of the signal and improve the signal-to-noise ratio of the vibration signal, while a six-axis acceleration gyro sensor is used to realize the complementary fusion of the posture solution; temperature compensation and BP neural network model are used to eliminate the abnormal fluctuation of the data when the barometric pressure sensor monitors the height. The system does not change the existing structure of an elevator and does not use the elevator manufacturer's interface. The sensors are highly integrated and adapted to each manufacturer's elevators, have convenient installation, do not require additional wiring, and use low-cost features, thus achieving remote monitoring of an elevator's operation status and automatic alarm for failures of an elevator.

2. Proposed Overall System Structure

A universal IoT system consists of three major parts, namely, the perception layer, the network layer, and the application layer. Among them, the perception layer is the "five senses" of an IoT system, which receives external information; transmits the perceived information to the IoT system, mainly through the relevant sensors; and collects the data required by the IoT system. The network layer is the host that transmits the information to the cloud through the network, which is equivalent to a human body's nerves; receives the information coming from the lower layer; and transmits it to the corresponding cloud according to the demand. The purpose of the application layer is to react according to the data according to the application written after receiving various information, or to send the corresponding commands on its own initiative, which is equivalent to the brain of a human body.

There are three main parts in this system: the sensor part, the microcontroller part, and the information management system part [23–25]. The system structure is shown in Figure 1.

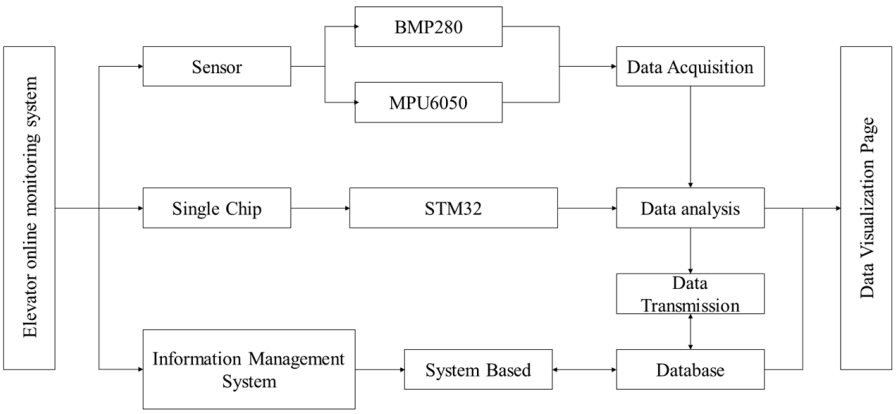

Figure 1. System structure.

Elevators may experience various failures during their everyday usage, such as component wear causing changes in the original precision of the parts, foreign objects obstructing elevator door components, and parts becoming loose due to external force impacts. There are many types of elevator failures, including elevator personnel entrapment accidents, elevator shearing accidents, elevator collision accidents, and elevator fall accidents. To prevent such mechanical failures, it is necessary for companies to focus on monitoring data, such as elevator door switches, elevator posture, and elevator height. This system specifically focuses on monitoring elevator posture data and elevator height data. The system is highly integrated with a six-axis acceleration gyroscope sensor, a barometric pressure sensor, and an STM32 minimum system to obtain the vibration signal of an elevator car, as well as its height signal, and the edge calculation processing is carried out by the microcontroller on the collected data so as to derive the relevant state information of the elevator car, which completes the collection of the relevant state information and ultimately realizes the diagnosis of the elevator's abnormal behavior. After completing the diagnosis, the basic information of the elevator and the diagnostic results are transferred to the database [26] through NB-IoT technology, in which time stamps are automatically added to the data for the subsequent visualization screen to retrieve the data according to the time. After completing the data transfer, the data visualization screen reads the data in the database, updates the data on the screen in real-time, and triggers an alarm automatically when there is a fault message. When there is a need to view historical data, the relevant data can also be retrieved and displayed on the visualization screen.

3. Hardware Design

According to the needs of the system, it is necessary to monitor the vibration acceleration, speed, and height information of an elevator car; analyze the posture information of an elevator car in real-time through the microcontroller system; carry out real-time monitoring and judgment on any relevant faults that may occur in an elevator; send the information to the Internet of Things platform through the Internet of Things module; and then carry out the design of the relevant hardware in response to the above requirements.

The structure of the hardware part of the system is shown in Figure 2. The hardware part of the device includes the STM32 main control chip, the barometric pressure sensor, the three-axis acceleration sensor, the NB-IoT module, and the power supply part. The barometric pressure sensor and the three-axis acceleration sensor collect the barometric pressure and acceleration data of an elevator car, and the STM32 main control chip processes the collected data and then packages the data to be transmitted to the IoT platform through the serial port and the NB-IoT module communication. After processing the collected data, the STM32 main control chip packages and transmits the data to the IoT platform through the serial port and NB-IoT module.

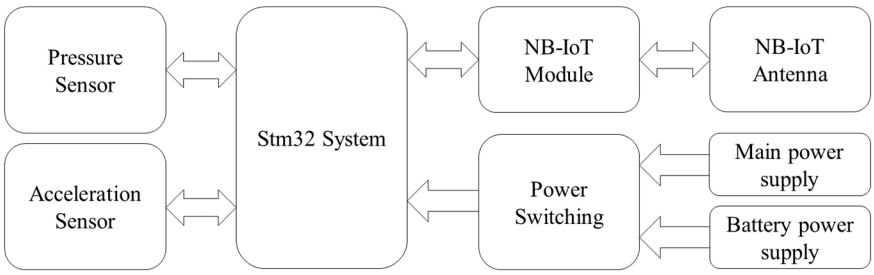

Figure 2. Block diagram of edge monitoring device hardware.

3.1. Introduction to the Main Controller Module

This system adopts an STM32F407VET6 MCU leverages ST's NVM technology and ART Accelerator™ as the main control chip (STMicroelectronics, Geneva, Switzerland). The core uses a 32-bit high-performance Arm® Cortex®-M4 processor (Arm, San Jose, CA, USA) with a clock frequency of up to 168MHz; supports FPU (floating-point arithmetic)

and DSP instructions; has three low-power modes of sleep, stop, and standby; and has abundant on-chip peripheral resources. The STM32 minimum system part includes an ISP one-button download circuit, a crystal oscillator circuit, and an SD card storage circuit.

3.2. Data Acquisition Module Design

3.2.1. Barometric Acquisition Module Design

The chip used in the Barometric Pressure Acquisition Module is BMP280, which can simultaneously acquire barometric pressure data and temperature data, and communicate data with STM32 through the IIC communication protocol. Due to its small size and low power consumption, it is suitable for application in watches, cell phones, and embedded devices, with a relative accuracy of ±0.12 hPa and an absolute accuracy of up to ±1 hPa. When the barometric sensor collects barometric data, it needs to be converted to altitude by the relevant code. The peripheral circuit design of the BMP280 is shown in Figure 3. The following notations are used: SDI—data signal; SCK—clock signal; C1 and C2 are filter capacitors; R1, R2, and R3 are pull-up resistors; R4 is a pull-down resistor.

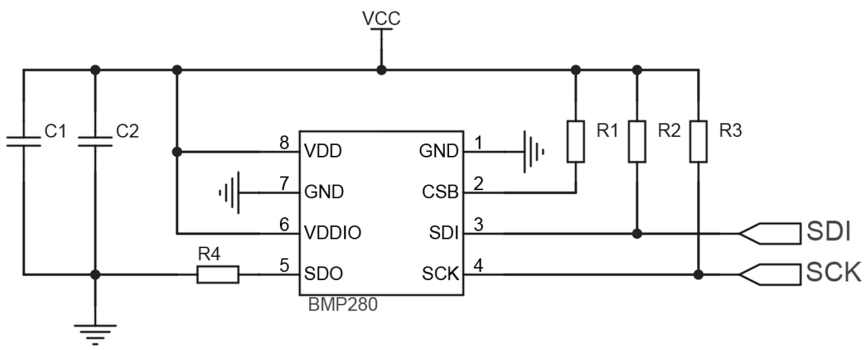

Figure 3. BMP280 peripheral circuit design.

Due to the barometric pressure being greatly affected by the environment, the size of the barometric pressure value is related to the height, temperature, and other conditions; with a change in temperature, the transformation of the barometric pressure will have a large gap. The barometric pressure value measured under the same height at different times of the day is converted to obtain the height difference, which can be up to hundreds of meters, and the difference in the barometric pressure values measured in different seasons will be even bigger, so it is necessary to introduce temperature data to correct the barometric pressure values. In this thesis, the hypsometric formula is used to correct the barometric pressure values by temperature, and compared with the barometric pressure–height formula, the measured altitude values are more accurate and less affected by temperature changes. The barometric pressure to altitude conversion formula is given below:

$$h = \frac{[(P_0/P)^{(1/5.257)} - 1] \times (T + 273.15)}{0.0065} \tag{1}$$

where P_0 is the standard atmospheric pressure, P_0 = 101.325 kPa, and T is the current air temperature.

A comparison of the calculated values of altitude without introducing temperature compensation and with temperature compensation added for barometric pressure sensors running for a long period of time is shown in Figure 4. When the barometric pressure sensor is operated for one thousand seconds without introducing temperature compensation, the barometric pressure value will change dramatically with the change in temperature at a constant height, which, in turn, will cause errors in height readings, as shown in Table 1. In the actual use of the elevator, the standard deviation and variance of the altitude sensor readings without temperature compensation are much larger than when temperature compensation is used, so the use of temperature compensation can effectively reduce the reading error when the elevator is running for a long time.

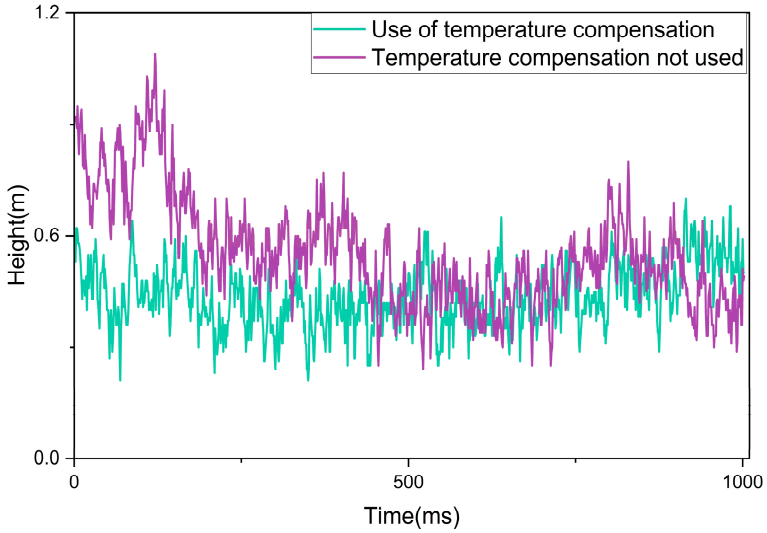

Figure 4. Comparison of height sensor readings.

Table 1. Actual height sensor readings.

	Average Value	(Statistics) Standard Deviation	Variance (Statistics)
Use of temperature compensation	0.4371	0.0835	0.0069
Temperature compensation not used	0.5531	0.1491	0.0222

3.2.2. Design of Six-Axis Acceleration Gyroscope Acquisition Module

The design uses an InvenSense® (San Jose, CA, USA)'s MPU6050 chip, which integrates a three-axis acceleration and three-axis gyroscope acquisition module, communicates with the SMT32 through the IIC communication protocol, simultaneously outputs the operating data of the three-axis acceleration and three-axis gyroscope, and utilizes the DMP module (Digital Motion Processor) inside the MPU6050 chip to solve the sensor data, transmit the posture data to the microcontroller, and reduce the computing power of the master controller. The peripheral circuit design of the MPU6050 chip is shown in Figure 5. The following notations are used: SDA—data signal; SCL—clock signal; C3, C4, C5 and C6 are filter capacitors; R5 and R6 are pull-up resistors; R7 is a pull-down resistor.

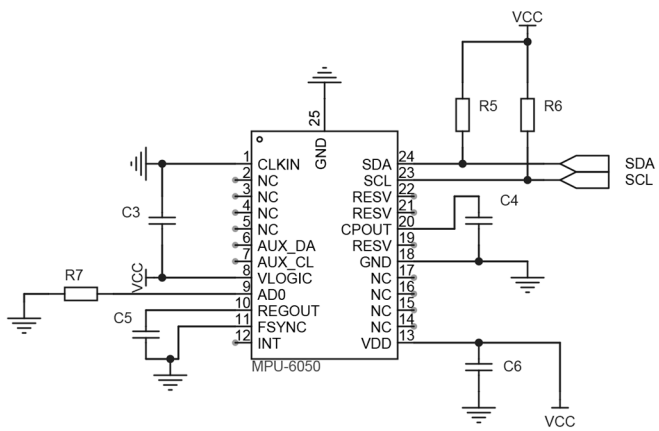

Figure 5. MPU6050 peripheral circuit design.

In this system, the MPU6050 chip is used to measure the elevator car posture, including rotation around the *x*-axis (roll angle), rotation around the *y*-axis (pitch angle), and rotation around the *z*-axis (heading angle yaw) [27,28]. Due to the use of the three-axis acceleration

data alone for the posture solution, it is not possible to calculate the heading angle. And the use of the three-axis gyroscope data to calculate the car posture alone, there is a need to integrate the angular velocity over time, and the data results gradually shift with the change in time; therefore, there is a need for the complementary fusion of the two calculated results to ultimately obtain accurate data.

3.3. NB-IoT Module Design

NB-IoT is built on a cellular network and can be directly deployed on the GSM network, UMTS network, or LTE network to reduce the deployment cost. This system utilizes the Fruit Cloud GA7 chip and STM32 for data transmission through the serial port, configures the NB-IoT module through AT commands, and directly connects to the IoT platform using the MQTT communication protocol to send the collected data within different subscription topics. NB-IoT technology can be utilized to link directly to the IoT platform through the existing base station to achieve a low-power wireless link in embedded devices. As the peripheral circuit of the IoT module has high signal transmission requirements, it is necessary to filter the ripple in the rectified output voltage as well as the electrostatic shielding, and it is necessary to complete the impedance matching of the antenna part to prevent the high-frequency circuit signals from reflecting back to the source point and to improve the energy efficiency. The peripheral circuit design of the NB-IoT module is shown in Figure 6. The following notations are used: MCU_RX and MCU_TX are used to connect to the serial port of the primary controller; SIM_VDD, SIM_DATA, SIM_CLK, and SIM_RST are used to connect to the SIM card; C7 is used to ensure chip voltage stability; C8 and C9 are filter capacitors; D1(Electro-Static discharge) prevents static electricity from affecting signals.

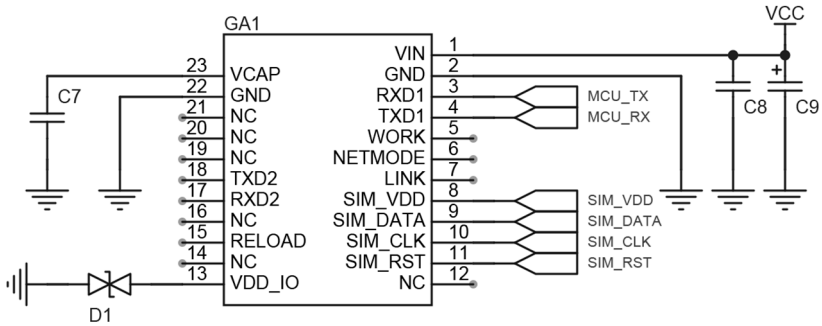

Figure 6. NB-IoT module peripheral circuit design.

3.4. Power Supply Module Design

According to the requirements of the Technical Specification for Remote Monitoring Devices for Elevators (Trial), the remote monitoring device should be equipped with an emergency power supply, and the remote monitoring device should be capable of storing and sending the status of the device before power failure, and at the same time, it should ensure that an elevator's image acquisition device works for at least one hour. Therefore, the elevator monitoring device must be continuously powered by the main power supply during normal operation and automatically switched to its own battery for continuous power supply when an elevator power failure occurs. The power supply module consists of three parts: a 12 V to 5 V step-down part, as shown in Figure 7a, F1 and D2 are used to protect the circuit, R8 is used for voltage division to ensure the stability of the '5VOUT' voltage in the figure, C10 and C11 are filter capacitors; a lithium battery boosting part, as shown in Figure 7b, VBAT-IN—battery input, VBAT-OUT—battery output, L1 and D3 guarantee voltage output, R9 and R10 are sampling resistors, C12 and C13 are filter capacitors; and a dual power supply automatic switching circuit, as shown in Figure 7c, three MOSFETs Q1, Q2 and Q3 are used to automatically switch power supply.

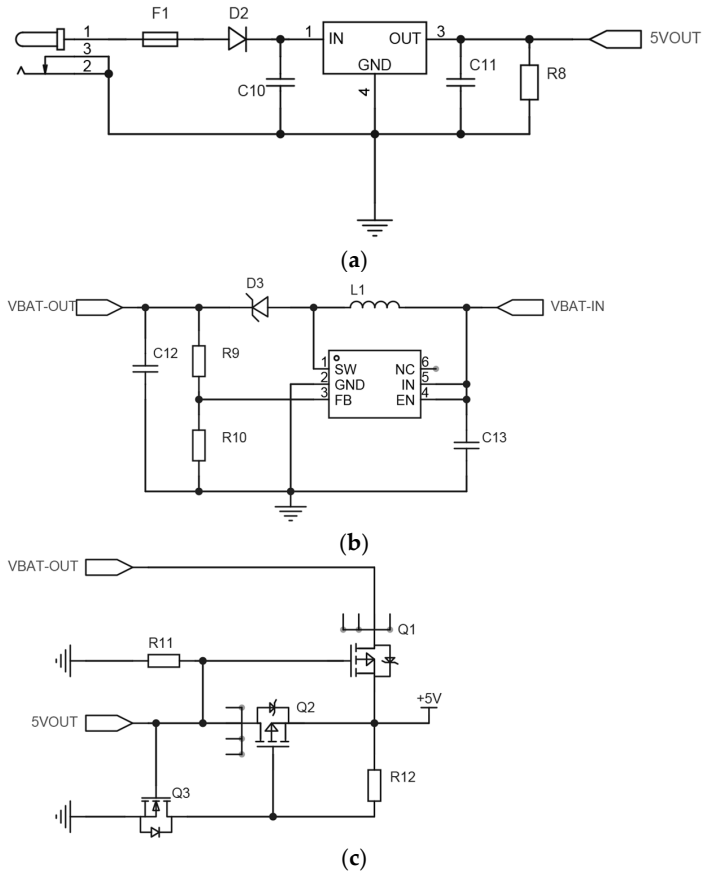

Figure 7. Circuit design of power supply section. (**a**) The 12 V to 5 V step-down circuits; (**b**) Li-ion battery boost circuitry; (**c**) dual power supply automatic switching circuits.

Among them, the 12 V to 5 V step-down circuit uses a 78M05 linear regulator, which is able to reduce the 12 V power supply from the external DC power input to 5 V; due to the 3.7 V lithium battery having different amounts of power, with a voltage range of 2.5 V–4.25 V, in order to ensure that it can stably output the 5 V voltage, the MT3608 power supply chip is used to increase the voltage. The output voltage is between 5.14 V and 5.142 V, the test results are shown in Figure 8, the circuit can automatically switch between the main and secondary power supplies when the two voltages are the same, and the main power supply is used to power the main power supply when the main power supply V1 is input, and when the main power supply V1 is disconnected, it is automatically switched to the external power supply V2 for power supply.

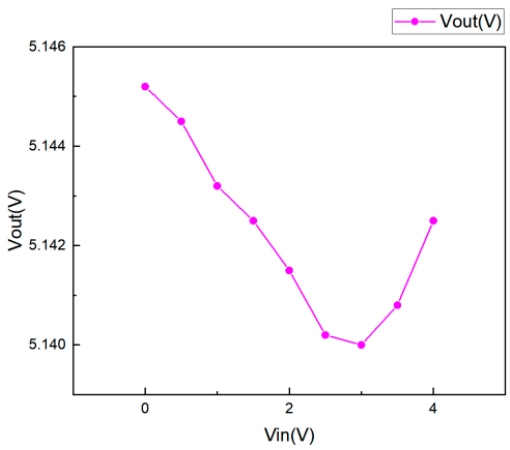

Figure 8. MT3608 operating characteristic curve.

4. Algorithm Design

4.1. Car Posture Fusion Solution

Since a posture solution using three-axis acceleration data alone cannot be calculated to obtain the heading angle, and using three-axis gyroscope data alone to calculate the car posture requires time integration of angular velocity, and the results of the data are gradually shifted over time, it is necessary to complement the results obtained from the two calculations by fusing them together to finally obtain valid data.

4.1.1. Accelerometer Solved Posture

When the sensor is stationary, the sensor itself has no acceleration data and is only affected by the acceleration of gravity; when the sensor's z-axis is vertically upward, the x and y directions are measured to obtain the value of 0. Only the z-axis is measured to obtain the acceleration of gravity, g. When the sensor is tilted at a certain angle, the acceleration of gravity will produce components in other directions, so the posture of the sensor can be obtained by calculating the rotation of the x, y, and z axes, and the specific calculation is:

$$\begin{bmatrix} a_x \\ a_y \\ a_z \end{bmatrix} = \begin{bmatrix} -\sin p \\ \cos p \cdot \sin p \\ \cos p \cdot \cos r \end{bmatrix} \cdot g \tag{2}$$

Solving the above equations yields the roll and pitch angles.

$$\begin{cases} roll = \arctan(\frac{a_y}{a_z}) \\ pitch = -\arctan(\frac{a_x}{\sqrt{a_y^2 + a_z^2}}) \end{cases} \tag{3}$$

4.1.2. Gyroscope-Solved Posture

By measuring the angular acceleration of the three axes and integrating the angular acceleration, the rotation angle of the three axes can be obtained. In this system, by integrating the angular acceleration per unit of time, the amount of change in rotation angle per unit of time can be obtained, and after accumulating with the initial amount, the posture of the sensor can finally be obtained. The conversion relationship between angular acceleration and angular velocity is given in the following equation:

$$\begin{bmatrix} g_x \\ g_y \\ g_z \end{bmatrix} = \begin{bmatrix} 1 & 0 & -\sin p \\ 0 & \cos r & \cos p \cdot \sin r \\ 0 & -\sin r & \cos p \cdot \cos r \end{bmatrix} \cdot \begin{bmatrix} \frac{dr}{dt} \\ \frac{dp}{dt} \\ \frac{dy}{dt} \end{bmatrix} \tag{4}$$

$$\begin{bmatrix} \frac{dr}{dt} \\ \frac{dp}{dt} \\ \frac{dy}{dt} \end{bmatrix} = \begin{bmatrix} 1 & \frac{\sin p \cdot \sin r}{\cos p} & \frac{\cos r \cdot \sin p}{\cos p} \\ 0 & \cos r & -\sin r \\ 0 & \frac{\sin r}{\cos p} & \frac{\cos r}{\cos p} \end{bmatrix} \cdot \begin{bmatrix} g_x \\ g_y \\ g_z \end{bmatrix} \tag{5}$$

where g_x, g_y, and g_z are the three-axis angular velocities obtained from the three-axis gyroscope measurements.

4.1.3. Posture Fusion

Based on the above analysis, it can be concluded that the heading angle yaw cannot be calculated using three-axis acceleration data alone, and using the three-axis gyro data alone will result in a drift after a long period of measurement, so it is necessary to perform posture fusion of the two sources of data.

$$\begin{cases} roll = roll + (roll_{acc} - roll_{gyro}) \cdot K \\ pitch = pitch + (pitch_{acc} - pitch_{gyro}) \cdot K \\ yaw = yaw_{gyro} \end{cases} \tag{6}$$

where K is the scale factor, which needs to be adjusted according to the actual situation, in this system, where $K = 0.4$.

4.1.4. Acceleration Signal Pulse Peak-to-Peak Algorithm

Even though the elevator acquires an effective posture, the vibration data still play a significant role in the smoothness of the elevator; therefore, during the process of acquiring the elevator vibration signals using the triaxial acceleration sensors, the range of variation in the vibration signals is reflected by the peak-to-peak values, which are calculated as shown in Equation (7). The interval estimation of the peak-to-peak values of the vibration and pressure pulsations under stable working conditions is as follows: For a given peak-to-peak value sample data (x_1, x_2, x_N), the mean value of the peak-to-peak value μ and standard deviation σ are calculated. For a given sample of peak values, the mean value and standard deviation of the peak values are given as $(\mu - 1.96\sigma, u + 1.96\sigma)$. That is, the probability that the peak value falls within the interval $(\mu - 1.96\sigma, u + 1.96\sigma)$ is 95%.

$$x_{p-p} = max(x_i) - min(x_i) \tag{7}$$

The condition monitoring in this paper utilizes quasi-periodic sampling, where the number of fixed sampling points in a rotational cycle is usually 2^n, where $n \in N$. n is between 6 and 12. For steady-state conditions at a fixed rotational speed, there is no significant difference between the data obtained from quasi-periodic sampling and a fixed sampling rate. To fully assess the applicability of the peak-to-peak algorithm, in the field test signals, the vibration of the unit obtained by the speed sensor contains a high-frequency component, the pendulum signal is generally low-frequency as the main frequency, and the pressure pulsation signal is rich in frequency components. According to the above method, the measured signals are sampled, the peak-to-peak values are calculated, and the results obtained are shown in Figure 9. In the figure, N indicates the number of points calculated per cycle, C indicates the number of cycles used, and P is the peak-to-peak value. By observing the figure, it can be found that the maximum values in the peak-to-peak calculation results are 99.73, 100.1, 100.06, 100, and 100, and there is no difference between the peak-to-peak calculation and the peak-to-peak calculation of a single-frequency sinusoidal signal without interfering noise, which indicates that the use of a larger confidence interval in the case of a large signal-to-noise ratio can yield more accurate results.

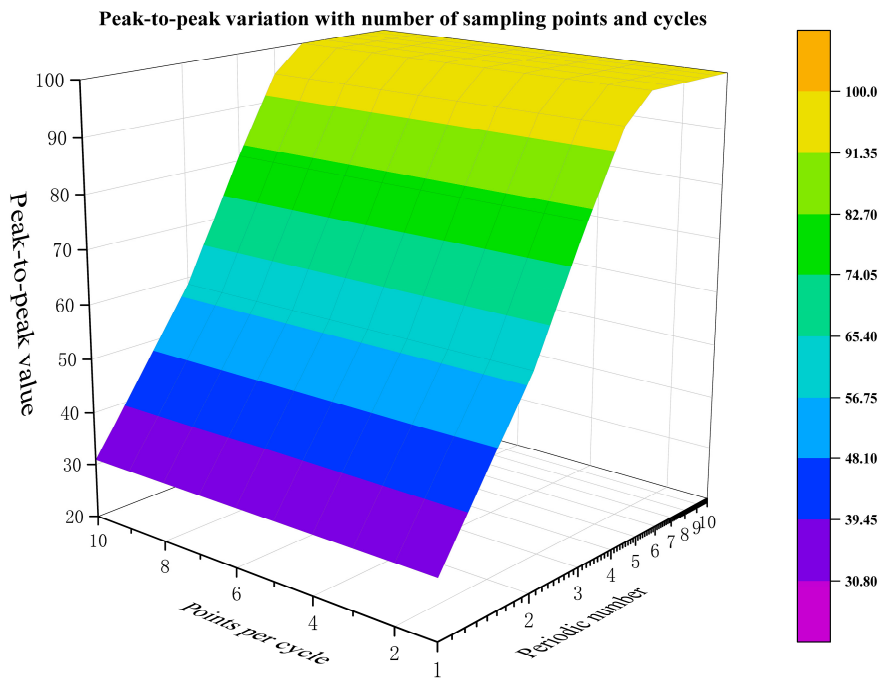

Figure 9. Variation in peak-to-peak values for MPU6050.

4.2. Barometric Sensor Zero Drift Height Error Compensation

Since barometric pressure sensors are susceptible to data fluctuations due to environmental influences, and barometric pressure sensors produce zero drift in a stable barometric pressure environment, in this paper, BP neural networks are trained to eliminate the effect of zero drift on height error.

4.2.1. Modeling and Training of BP Neural Networks

A BP (back propagation) neural network is a multi-layer feed-forward neural network trained according to the error back propagation algorithm, which is one of the most widely used neural network models. A BP network can learn and store many input–output pattern mapping relationships without revealing the mathematical equations describing such mapping relationships beforehand, and it can classify arbitrarily complex patterns and has excellent multi-dimensional function mapping ability.

A typical BP neural network topology consists of input, hidden, and output layers, as shown below.

As shown in Figure 10, X_1 to X_i are the data in the input layer, which are the inputs of information and transmit the data to the subsequent hidden layer; ω_{ij} are the weights of the input layer neurons transmitting the data to the hidden layer neurons; ω_{ik} are the weights of the hidden layer neurons transmitting the data to the output layer neurons; and Y_1 are the activation functions of the output data hidden layer and output layer using tan-sigmoid and purelin functions, respectively. The hidden layer can be single or multi-layer; theoretically, if there are enough hidden neurons, the BP neural network can approximate any nonlinear mapping.

According to the previous data, it can be seen that the data input to the BP neural network contains two-dimensional feature vectors of time data and temperature data, the input layer of the neural network is set to be two neurons, the barometric pressure value under the current time is predicted by the neural network to compensate for the temperature and the zero drift, the output value of the neural network is set to be the barometric pressure value, and the output layer of the neural network is set to be one neuron. Since the number of neurons in the hidden layer is very important for the final training results of the neural network, and an inappropriate number of neurons in the hidden layer will produce a large error in the training results of the neural network, the reference value is, therefore, usually calculated by the empirical Formula (8), and then, the number of neurons is finally determined by the experimental method.

$$h = \sqrt{a + b} + c \tag{8}$$

where h is the calculated reference value, a and b are the number of neurons in the input layer and the number of neurons in the output layer, respectively, and c is an adjustable parameter in the range of 2–10.

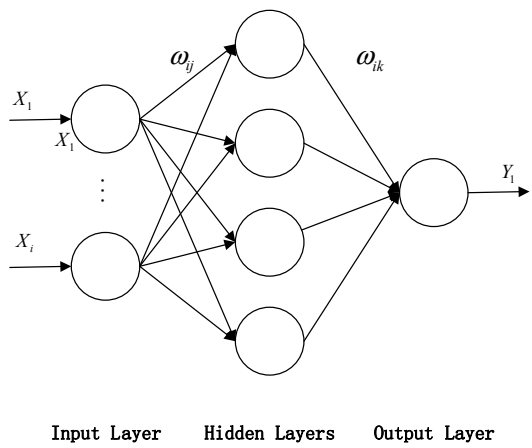

Figure 10. Topology of BP neural network.

4.2.2. Neural Network Training

After many experiments, when the number of neurons in the hidden layer is eight, the root-mean-square error of the training set is the smallest and the convergence speed is the fastest; therefore, the best results can be achieved using a neural network with the structure 2-8-1, and the structure of the established neural network model is shown in Figure 11.

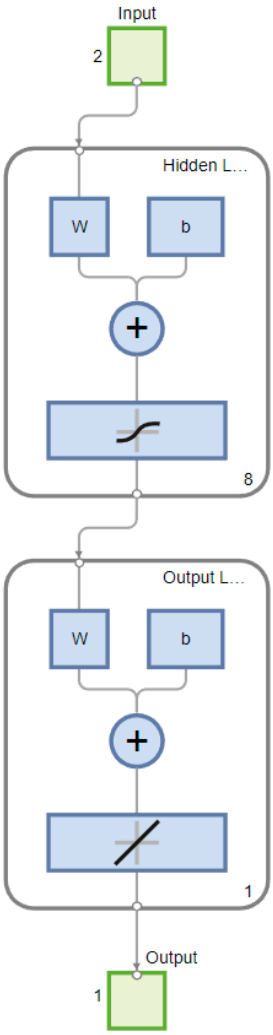

Figure 11. Structure of BP neural network.

4.2.3. Analysis of Experimental Results

The best performance is obtained when the number of training sessions is two, whereby the mean square error is 0.017321, as shown in Figure 12.

The test set samples are fed into the neural network to calibrate the training results and the test results obtained, as shown in Table 2.

From the data in Table 2, it can be concluded that the error between the actual results and the predicted results is small, and the proposed model can more accurately predict the temperature drift and zero drift generated by the change in barometric pressure with time and temperature, which can eliminate the influence of the two on the measurement results of the sensor. Among them, Figure 13 shows the fitting effect of the training set, validation set, and test set for the actual output, from which it can be seen that the correlation coefficients R of the training set, validation set, and test set are 0.9812, 0.95389, and 0.98928, respectively, and the overall correlation coefficient reaches 0.98003, which shows that the completed BP neural network model has a better fitting degree, and the time–temperature two-dimensional vector deduced from inputs is more accurate. The

time–temperature two-dimensional vector inference for height data and the actual height data deviation are small, indicating that the elimination of the barometric pressure sensor's zero drift error has a good effect.

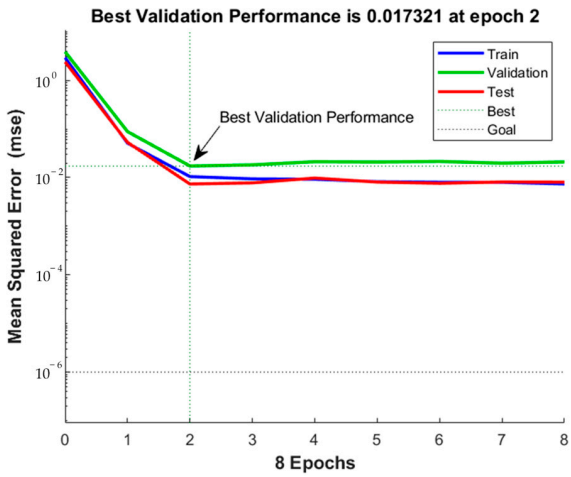

Figure 12. Iteration diagram of BP neural network.

Table 2. Test sample output results.

Serial Number	Actual Value	Projected Value	Inaccuracies
1	264.4232	264.6375	0.2143
2	264.3950	264.7516	0.3566
3	264.1141	264.2437	0.1296
4	263.8887	264.0049	0.1162
5	263.7196	264.3994	0.2797
6	263.8887	264.0553	0.1666
7	263.9450	264.1020	0.1570
8	264.2541	264.1422	−0.1119

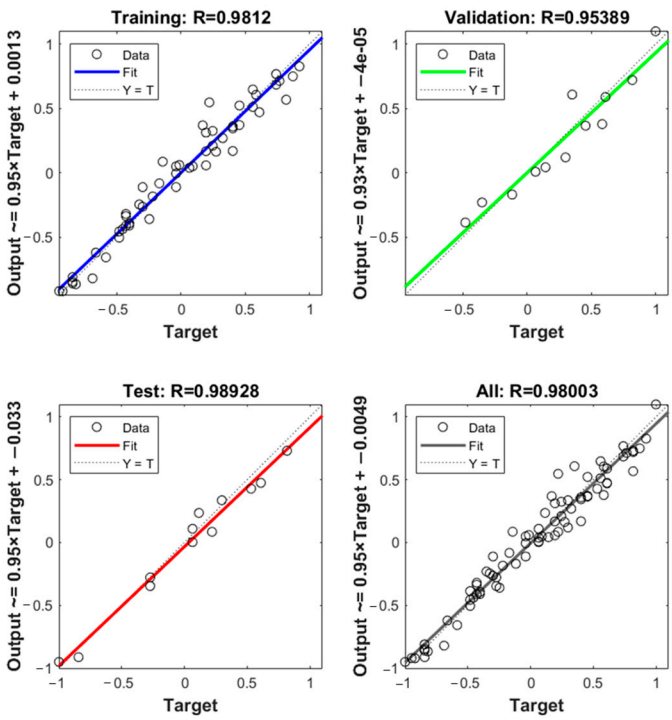

Figure 13. BP neural network fitting results.

5. Main Program Design

The main program design of the microcontroller mainly includes reading the data from the barometric pressure sensor, three-axis acceleration sensor, and three-axis gyroscope sensor; solving the car posture, vibration data, and the height calculated by temperature compensation through hardware DMP; completing the diagnosis of possible faults of the elevator car; and transmitting the data to the IoT platform through the IoT module. A flowchart of the program is shown in Figure 14.

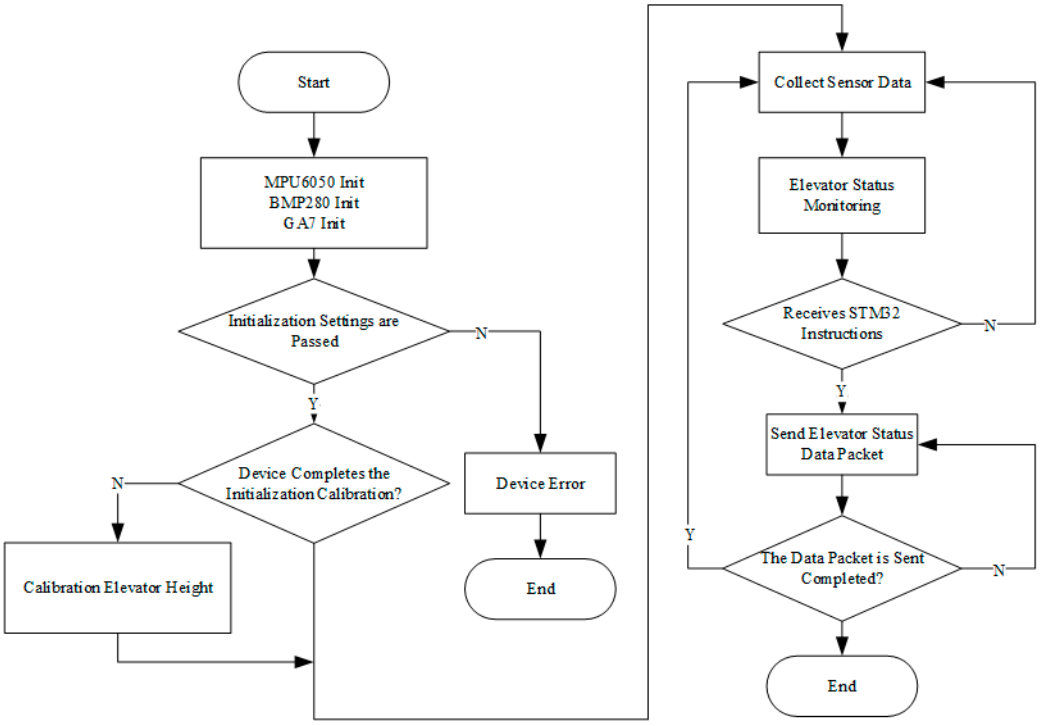

Figure 14. Main program flow.

5.1. Data Transmission Component

The data transmission process of this program uses MQTT v3.1.1 as the transmission protocol. MQTT is a client–server-based message publish/subscribe protocol, which is characterized as lightweight, simple, open, and easy to implement, and therefore is widely used in IoT devices. In MQTT protocol communication, the two sides of the communication are divided into the server and the client, in which the MQTT server's main function is to receive information sent by the client and also send information to the MQTT client; in addition, the server is also responsible for managing the MQTT client, which is needed to ensure that the communication is smooth and that the information is correctly accepted and accurately delivered. The client, on the other hand, is able to send information to the server and also receive information from the server. The process in which the client establishes a connection with the server includes creating a client, opening a client connection, creating a connection, subscribing to topics, and publishing data.

5.2. Real-Time Elevator Speed Monitoring

The elevator running speed command curve is shown in Figure 15. It can be divided into the following stages: the initial section of startup acceleration (AE section), the uniform acceleration section (EF section), the end of startup acceleration (FB section), the section of uniform motion (BC section), the initial section of deceleration motion (CF′ section), the section of uniform deceleration (F′E′ section), and the end of deceleration motion (E D). The main control board of the elevator actively sends elevator operation commands to control the running speed of the elevator. When the elevator speed is abnormal, it will

make the elevator operation deviate and lead to elevator leveling faults, so it is necessary to monitor the running speed of the elevator, and when the real-time speed of the elevator does not correspond to the commands, it is necessary to alert the faults to the cloud platform according to the elevator running stage.

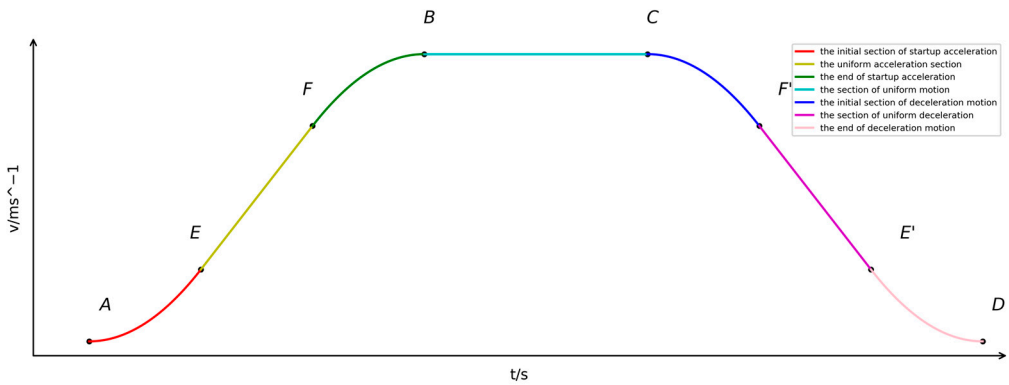

Figure 15. Elevator operation speed command curve.

5.3. Real-Time Data Transmission

Real-time data monitoring of the elevator is very important for the daily operation and maintenance of the elevator. The sampling frequency of the sensor of this system is 100 hz; in order to avoid the influence of the sensor's error on the collected data, it adopts five consecutive sampling points to seek the average value as a valid sampling point, which, together with the filtering algorithm inside the sensor, greatly reduces the error of the collected data of this system. The collected real-time speed data, front and rear offset of the elevator car, left and right offset, the number of times the elevator goes up and down, the elevator running distance, and other data are packaged and sent to the IOT platform according to the frequency of once per minute.

6. Experimental Validation

In order to verify the procedures established in this paper, the production of the equipment was completed through self-welding, as shown in Figure 16. The experiment was conducted on an elevator manufactured by Xizi Otis Elevator Co., Ltd. (Hangzhou, China), in Building C of the Beijing University of Civil Engineering and Architecture. This equipment was purchased in Suzhou, Jiangsu Province, China.

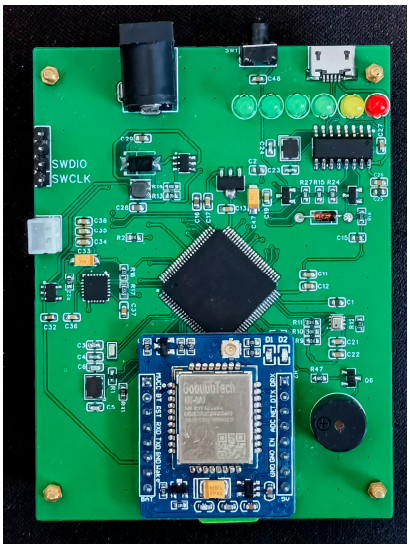

Figure 16. Physical equipment.

6.1. Validation of Six-Axis Acceleration Gyroscope Posture Monitoring

This system also monitors the posture of the elevator during operation. The data from the running posture during elevator operation are very important. If the offset is too large during the operation of the elevator, it will lead to excessive wear and tear of the elevator guide rail, which will affect the normal operation of the elevator, and the vibration will be increased during daily operation. As shown in Figures 17 and 18, the offset of the elevator in the horizontal and vertical directions can be accurately detected during the operation of the elevator.

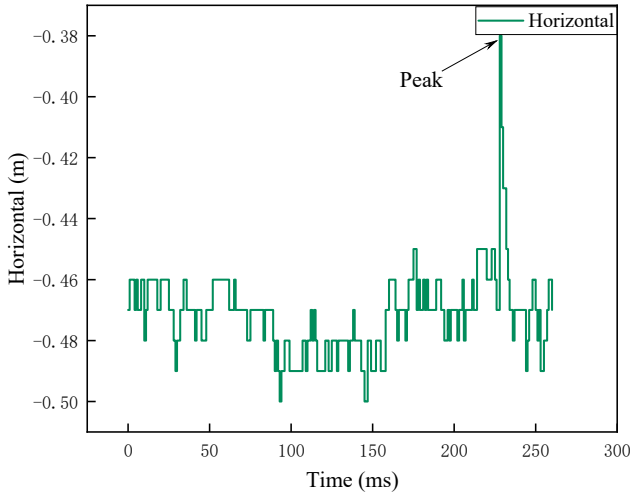

Figure 17. Horizontal offsets during elevator operation.

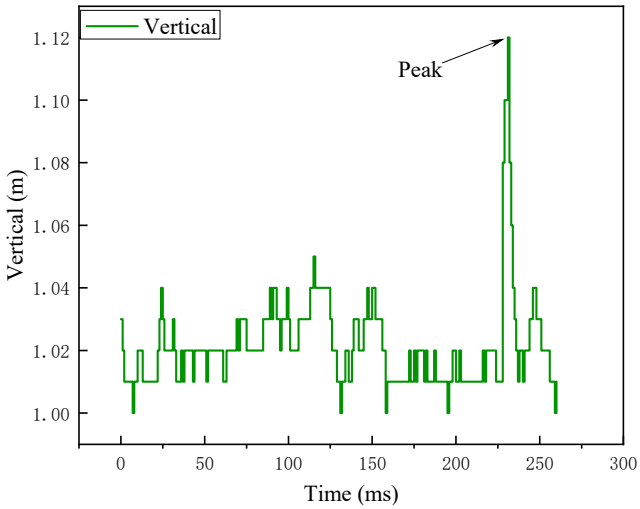

Figure 18. Vertical offset during elevator operation.

In the monitoring process, from the data measured in Table 3, it can be seen that during the monitoring process of vertical offset and horizontal offset, when the elevator experiences sudden vibration, it can be monitored whether the elevator posture undergoes a sudden change. The amplitude of vibration is less than 0.2°. Through many experiments, it can be obtained that the three-axis acceleration and three-axis gyroscope sensors monitor the elevator car posture and meet the accuracy requirements, and the monitoring data are stable, so it can be determined that there is no abnormal vibration in the elevator operation process, and the elevator works normally.

Table 3. Statistical results of front and rear offsets.

Experiment Number	Test Items	Mean Value/°	Peak/°
First	Vertical offsets	1.021	1.122
	Horizontal offsets	−0.471	−0.381
Second	Vertical offsets	1.003	1.103
	Horizontal offsets	−0.483	−0.389
Third	Vertical offsets	1.032	1.135
	Horizontal offsets	−0.478	−0.392

6.2. Validation of the Method for Calculating Peak-to-Peak Values under Confidence Intervals

In order to verify the effectiveness of the peak-to-peak value algorithm proposed in this paper under a 95% confidence interval with noise-containing conditions, 10 groups of elevator car vibration signals were collected with personnel walking in the car. The vibration signal was superimposed on Gaussian white noise at −1 dB. Figure 19 shows the time-domain waveforms of one group of signals, blue waveforms for the clean vibration signals, and red curves for the vibration signals superimposed on the noise, and it can be observed that the peak-to-peak value is 0.165. The traditional method and the method proposed in this paper are used to calculate the signal, as shown in Figure 20. The peak-to-peak value is 0.165. The peak-to-peak value of the signal is calculated using the traditional method and the method proposed in this paper, as shown in Figure 20, from which it can be seen that the peak-to-peak value of the vibration signal fluctuates greatly under noise interference and the credibility of the calculation result is low; based on the method proposed in this paper, the peak-to-peak value is stable in a small interval, which proves that this paper's method has the ability to obtain an accurate peak-to-peak value under noisy conditions. Thus, it can be inferred that the peak-to-peak value algorithm under the 95% confidence interval can accurately extract the vibration signal to judge the vibration state of the elevator.

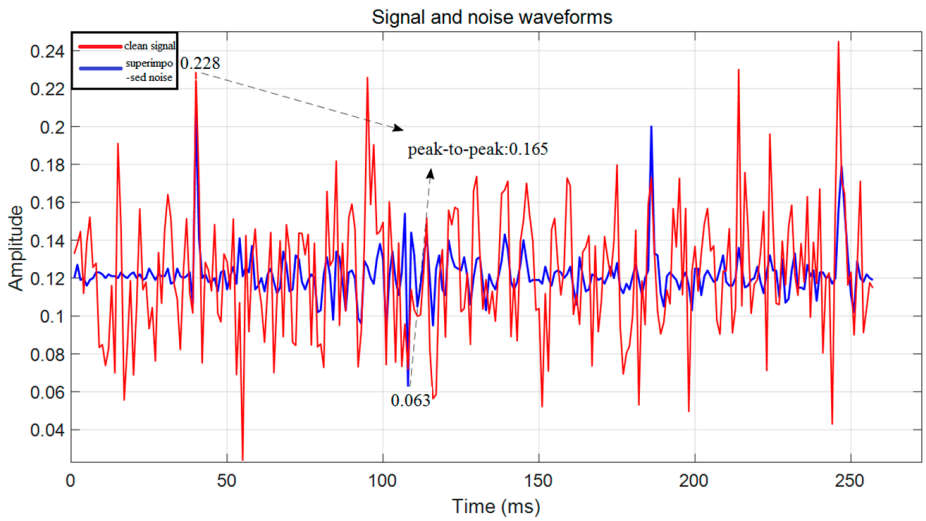

Figure 19. Vibration signal of people walking in the car.

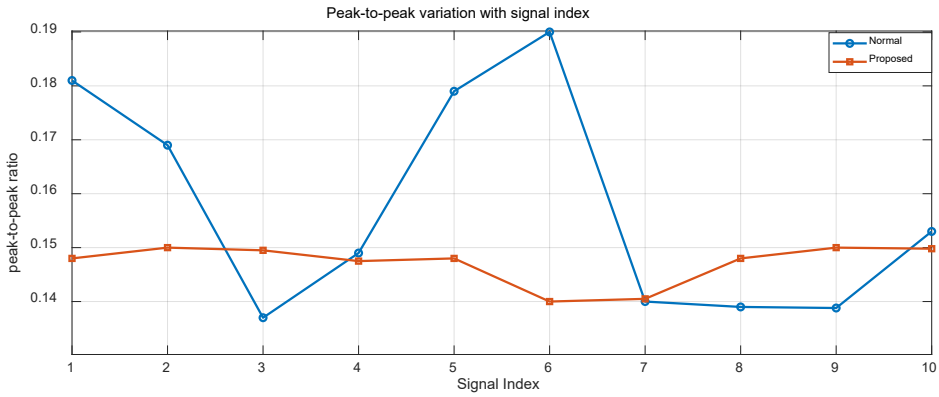

Figure 20. Comparison between traditional peak-to-peak algorithm and peak-to-peak algorithm with 95% confidence interval.

6.3. Validation of Barometric Sensor Height Monitoring

Here, we verify the corrective effect of the BP neural network training model on the barometric pressure sensor. Firstly, the air pressure sensor is used to measure the air pressure value of the first floor, and the air pressure value of the first floor is used to zero. Then, the height difference is obtained according to the subsequent measurement of the air pressure value, the floor height is 3.5 m, and the measurement results are shown in Table 4.

Table 4. Statistical results of data.

Actual Floor	Actual Relative Height/m	Measured Relative Height/m	Height Error/m
1	-	0	0
2	3.5	3.3814	−0.1186
3	7	7.1359	+0.1359
4	10.5	10.6824	+0.1824

According to the experimental results, it can be obtained that the relative height obtained after temperature correction and the actual height error is within ±20 cm, and the leveling accuracy meets the design requirements of this system, and during the experiment, all data are accurately transmitted to the cloud server.

6.4. Overspeed Monitoring Validation

By monitoring the displacement per unit time in the direction of the elevator Z-axis, the height difference is used to carry out the calculation of real-time elevator speed. According to GB/T 10058-2009 [29], the overspeed protection device of the elevator car should be able to monitor the speed loss control of the car, the lower limit of which is 115% of the rated speed of the elevator, so 115% of the rated speed of the elevator is set as the threshold of overspeed of the elevator, and the test is carried out by using the elevator's fast-running gear, the rated speed of the elevator is 1.5 m/s. The elevator is found to be able to effectively complete the fault determination of the elevator's overspeed, and the results of its monitoring and verification are shown in Table 5.

Table 5. Statistics on speeding monitoring.

Test Serial Number	Actual Results/$(m \cdot s)^{-1}$	Ratio to Rated Speed	Is It Speeding?
1	1.463	97%	No
2	1.634	109%	No
3	1.962	131%	Yes

7. Conclusions

In this paper, for the difficult problem of elevator fault monitoring, an NB-IoT-based elevator online monitoring system is designed, which is highly integrated with the sensor and microcontroller, to realize a low-cost, easy-to-install, and highly reliable elevator monitoring solution, and at the same time, the system uses six-axis sensors for posture determination and a high degree of error compensation for the zero-point drift in barometric pressure sensors, thus realizing the accurate transmission of data, which reduces the occurrence of false alarms for faults. The findings of this study mainly include the following:

(1) The related hardware design, including the MCU peripheral circuit design, sensor peripheral circuit design, NB-IoT module peripheral circuit design, power supply, and power switching circuit design, ensures that the edge monitoring equipment operates stably for a long period of time, as well as continues to operate normally in the event of a power failure.
(2) We use the complementary fusion of three-axis acceleration and three-axis gyroscope sensors, as three-axis acceleration sensors cannot calculate the heading angles and three-axis gyroscope sensors need to carry out time integration of the angular velocity, to ensure monitoring accuracy; at the same time, the peak-to-peak value of the signal is calculated using the 95% confidence interval algorithm to alleviate the suppression of noise on the high-frequency components of the vibration signal, which has the advantages of strong robustness and insensitivity to noise, ensuring that the signal has a large signal-to-noise ratio, thus obtaining more accurate elevator car posture and vibration operation data.
(3) By applying neural network model data training, the height error generated by the zero drift of the barometric pressure sensor is eliminated, thus realizing the accurate judgment of elevator height.

This system still needs to be perfected in terms of elevator monitoring, and further research will be carried out in the future for the accurate judgment of the elevator switching door status, the image processing of elevator monitoring, and the internal monitoring of the elevator car.

Author Contributions: Conceptualization, Z.L. and J.N.; methodology, J.N. and T.L.; software, Z.L. and J.N.; validation, Z.L., J.N. and T.L.; formal analysis, Z.L.; investigation, Z.L.; resources, Z.L.; data curation, T.L.; writing—original draft preparation, J.N.; writing—review and editing, Z.L.; visualization, T.L.; supervision, T.L.; project administration, Z.L.; funding acquisition, Z.L. All authors have read and agreed to the published version of the manuscript.

Funding: This research received no external funding.

Institutional Review Board Statement: Not applicable.

Informed Consent Statement: Not applicable.

Data Availability Statement: Data are contained within the article.

Conflicts of Interest: The authors declare no conflicts of interest.

References

1. State Administration for Market Regulation. Circular of the General Administration of Market Supervision on the Safety Condition of National Special Equipment in 2021. *China Spec. Equip. Saf.* **2022**, *38*, 1–4.
2. Sun, H.; Chen, L.; Li, C. Design of wireless monitoring system for pump group based on internet of things. *Mech. Des. Manuf.* **2022**, *374*, 156–159.
3. *GB/T 6075.5-2002*; Measurement and Evaluation of Mechanical Vibration of Machines on Non-Rotating Parts Part 5: Hydroelectric Power Plants and Pumping Station Units. China Standard Press: Beijing, China, 2002.
4. *GB/T 11348.5-2008*; Measurement and Evaluation of Radial Vibration of Rotating Machinery Rotor Shafts Part 5: Hydroelectric Power Plants and Pumping Station Units. China Standard Press: Beijing, China, 2008.
5. *ISO 10816-2000*; Mechanical Vibration-Evaluation of Machine Vibration by Measurements on Non-Rotating Parts: Part 5. Machine Sets in Hydraulic Power Machine Sets in Hydraulic Power Generating and Pumping Plants. ISO: Geneva, Switzerland, 2002.

6. *ISO 20816-5-2018*; Mechanical Vibration—Measurement and Evaluation of Machine Vibration—Part 5: Machine Sets in Hydraulic Power Generating and Pump-Storage Plants. ISO: Geneva, Switzerland, 2016.
7. Zhang, F.; Ge, X.; Pan, L. Research on the calculation method of peak and peak values of main shaft oscillation of hydroelectric units under steady state working condition. *Vib. Shock* **2015**, *34*, 170–174.
8. Zhang, F.; Fu, J.; Fan, Y. EMD-based load shedding spindle oscillation of hydropower units. *J. Drain. Irrig. Mach. Eng.* **2017**, *35*, 863–868.
9. *GB/T 17189-2017*; Field Test Protocol for Vibration and Pulsation of Hydraulic Machinery (Hydraulic Turbines, Storage Pumps and Pump Turbines). China Standard Press: Beijing, China, 2017.
10. *IEC 60994-2017*; Guide for Field Measurement of Vibrations and Pulsations in Hydraulic Machines (Turbines, Storage Pumps and Pumpturbines). IEC: Geneva, Switzerland, 2017.
11. *ISO 20816-2017*; Part 2: Land-based Gas Turbines, Steam Turbines and Generators in Excess of 40 MW, with Fluid-Film Bearings and Rated Speeds of 1 500 r/min, 1 800 r/min, 3 000 r/min and 3 600 r/min. ISO: Geneva, Switzerland, 2018.
12. Liu, S.; Han, S.; Li, W. Research on elevator operation state monitoring and fault remote alarm system. *Autom. Instrum.* **2011**, *26*, 42–46.
13. Wang, E.; Hua, C.; Chen, J. Design of custom communication protocol elevator monitoring system based on STM32F103ZET6. *China Saf. Prod. Sci. Technol.* **2016**, *12*, 160–165.
14. Chen, Z.; Wang, Z. Research on elevator fault diagnosis and prediction based on big data. *Mech. Electr. Eng.* **2019**, *36*, 90–94.
15. Yang, Y.; Wang, Q.; Li, X. A non-intrusive intelligent monitoring method for elevator operation status. *J. Taiyuan Univ. Technol.* **2021**, *52*, 920–927.
16. Zhang, M.; Chen, C.; Huang, H. Design of real-time monitoring system for elevator based on internet of things. *China Test* **2012**, *38*, 101–105.
17. Sun, Y. Design of elevator acceleration monitoring system based on cloud platform. *Noise Vib. Control* **2018**, *38*, 474–476.
18. Xu, J.; Xu, L.; Wang, H.; Zheng, B.; Tang, B. Research on elevator condition monitoring technology based on vibration analysis. *Mech. Electr. Eng.* **2019**, *36*, 279–283.
19. Hao, J.; Xu, J.; Bao, C. Research on fault diagnosis of elevator drum brake based on VMD and SVM. *Electromech. Eng.* **2022**, *39*, 112–119.
20. Zheng, B.; Xu, J.; Wang, H. Research on thermal response characteristics of elevator inverter based on infrared thermal imaging. *Electromech. Eng.* **2019**, *36*, 418–421+439.
21. Nakanishi, H.; Kanata, S.; Sawaragi, T. GPS-INS-BARO hybrid navigation system taking into account ground effect for autonomous unmanned helicopter. In Proceedings of the 2012 IEEE International Symposium on Safety, Security, and Rescue Robotics (SSRR), College Station, TX, USA, 5–8 November 2012; pp. 1–6.
22. Matyja, T.; Stanik, Z.; Kubik, A. Automatic correction of barometric altimeters using additional air temperature and humidity measurements. *GPS Solut.* **2024**, *28*, 40. [CrossRef]
23. Lin, H.C.; Chou, F.Y.; Hong, Y.X.; Wang, Y.W. Fast Elevator Vibration Signal Cloud Collection System Using Data Compression and Encryption Algorithms. *Sens. Mater.* **2022**, *34*, 2311–2324. [CrossRef]
24. Olalere, I.O.; Dewa, M. Early fault detection of elevators using remote condition monitoring through IoT technology. *S. Afr. J. Ind. Eng.* **2018**, *29*, 17–32. [CrossRef]
25. Song, H.; Wang, Y.; Yang, F. Design and realization of smart gas meter system based on narrowband IoT. *Sens. Microsyst.* **2019**, *38*, 113–116.
26. Shen, Z.; Liang, J.; Yang, M. Design of elevator monitoring system based on LoRa and STM32. *Sens. Microsyst.* **2022**, *41*, 102–105.
27. Hao, Z.; Ge, W.; Hao, J. Research on embedded elevator operation state monitoring system. *J. Electron. Meas. Instrum.* **2019**, *33*, 187–193.
28. Dangana, M.; Ansari, S.; Abbasi, Q.H.; Hussain, S.; Imran, M.A. Suitability of NB-IoT for indoor industrial environment: A survey and insights. *Sensors* **2021**, *21*, 5284. [CrossRef] [PubMed]
29. *GB/T 10058-2009*; Specification for Electric Lifts. Chinese Standard: Beijing, China, 2009.